replication in cancer cells in metastatic lymph nodes, which in turn could be imaged with GFP fluorescence. Moreover, the finding that OBP-401 did not express GFP fluorescence in a mouse para-aortic lymphadenitis model induced by inoculating complete Freund adjuvant into the rectum submucosa of immunocompetent BALB/c mice suggests that this strategy could distinguish cancer metastasis from inflammatory lymphadenopathy (**Supplementary Fig. 4** online).

DISCUSSION

Lymph node status provides important information for both the diagnosis and treatment of human cancer[21, 22]. Lymphatic invasion is one of the major routes for cancer cell dissemination, and adequate resection of locoregional lymph nodes is required for curative treatment in patients with advanced malignancies. The risk of having lymph node metastasis can be partially predicted by clinical data such as tumor stage, serum tumor marker level, and medical images; there are, however, no noninvasive approaches to accurately predict the presence of lymph node metastasis, in particular, microscopic metastasis.

The specific aim of the present study was to determine the suitability of telomerase-specific amplification of the *GFP* gene for real-time imaging tumor tissues and, if so, detect nodal metastasis *in vivo* prior to the traditional, cumbersome procedures of histopathological examination. GFP-based fluorescence imaging can

allow real-time detection of target cells without time-consuming steps such as fixation and tissue processing[13-15]. Indeed, Yang *et al.* have shown that GFP-expressing tumors growing and metastasizing in intact animals could be viewed externally with a whole-body optical imaging system[13]. Moreover, the *GFP* gene could be delivered to metastatic tumor cells *in vivo* by viral vectors[14].

To distinguish normal from neoplastic tumor tissues, selective labeling of tumor cells is required. OBP-401 produced a viral yield of 6-7 logs in human cancer cells within 3 d of infection, which was 3-4 logs higher than that in normal cells, suggesting the reliable tumor selectivity of OBP-401. Although the reason why OBP-401 replicated slightly in NHLF despite of the lack of *hTERT* mRNA expression is unclear, the fact that NHLF could be maintained in the culture up to passages 10-20 indicates that NHLF might have a weak telomerase activity that is undetectable by standard PCR assay. However, the attenuated replication property of OBP-401 in normal cells seems not to interfere with the visualization of tumor cells *in vivo*. In fact, we detected no GFP expression in adjacent normal tissues in subcutaneous human cancer xenografts following intratumoral injection of OBP-401, although the cross-sections of the tumor were entirely imaged with GFP fluorescence. Thus, OBP-401 provides possible probing of tumor cells *in vivo*.

Experiments using a 3-CCD optical imaging system demonstrated that metastatic lymph nodes could be detected at laparotomy in mice 5 d after OBP-401 injection into implanted primary human rectal tumors. Of interest, metastatic lymph

nodes were imaged in spots with GFP fluorescence, which coincided with histologically confirmed micrometastasis. This experiment mimics the clinical scenario where patients with gastrointestinal malignancies with lymph node metastasis undergo surgery, and the data suggest that the surgeon can identify metastatic lymph nodes by illuminating the abdominal cavity with a Xenon lamp. The sensitivity and specificity of this imaging strategy are 92.3% and 86.6%, respectively, which are sufficiently reliable to support the concept of this approach. In our phase I trial of a replication-deficient adenovirus vector expressing the wild-type *p53* gene (AdCMV-*p53*, ADVEXIN), DNA-PCR analysis targeting the viral genome indicated that the virus was present in tumor tissue as well as proximal lymph nodes, suggesting regional spread of the vector via the lymphatic vessels[23]. Therefore, OBP-401 is likely to be accessible to the regional lymph nodes via intratumoral administration in humans.

Currently, analysis of lymph nodes with hematoxylin and eosin staining and microscopic examination usually involves review of only one or two tissue sections, and small foci of tumor cells can be missed. For intraoperative frozen section analysis of SNLs, this underestimation is even more pronounced due to poor tissue architecture. In the treatment of breast cancer and melanoma, in which SLN biopsy is commonly used, the sensitivity of intraoperative frozen-section analysis ranges from 38% to 74%[6-9]. In our experiments, additional serial sectioning was needed in 4 of 12 (33.3%) lymph nodes with GFP fluorescence to detect micrometastasis. This finding suggests

that this GFP-based approach has higher sensitivity for detecting occult lymph node metastasis compared to standard histopathological examination. Thus, the two GFP-positive nodes, in which tumor cells were not detected histologically, could have contained microscopic metastasis that would have been identified by further sectioning. Other possible explanations of false-positive detection include either that GFP protein itself was produced in the primary tumor spread into regional lymph nodes or that high doses of OBP-401 entered nodes and incidentally replicated in normal lymphocytes as they have low telomerase activity[24].

Although the molecular imaging strategy using OBP-401 is considered promising, some limitations of the system exist, the main one being the relatively short wavelength of excitation light of GFP. In contrast to luciferase that is also commonly used for molecular imaging[25], if objects are located in the deep layer or covered with thick adjacent tissues, the excitation light for GFP may not be able to reach them. For example, when tumor foci were exposed to the surface of nodes opposite the illuminated field, GFP fluorescence could not be detected, thereby leading to false-negative detection. The extension of exposure time to the illumination allows increasing the fluorescence intensity; the excitation light, however, cannot penetrate deeper. To raise the imaging sensitivity, one possible approach is to make the specimen thinner, for example, by pressing the excised lymph nodes flat; the architecture of the nodes, however, may be destroyed. Alternatively, it might be useful to develop a hand-held probe, in which the outlet of the excitation beam light and the

sensor of GFP fluorescence are combined. During surgery, metastatic lymph nodes could be positively identified with GFP fluorescence guided by this probe like a gamma probe for SNL biopsy. At least, a hand-held flashlight to excite GFP fluorescence has been previously reported[26].

Administration of OBP-401 can provide an additional advantage in cancer therapy. OBP-401, similar to OBP-301, is an oncolytic virus, and selectively kills human tumor cells by viral replication; the process of cell death by OBP-401, however, is relatively slow compared to apoptosis-inducing chemotherapeutic drugs, because the virus needs time for replication. Therefore, tumor cells infected with OBP-401 express GFP fluorescence, followed by loss of viability, allowing the timing of detection. We could speculate that OBP-401 would spread into the regional lymph nodes after intratumoral injection, express GFP signals in tumor cells by virus replication, and finally kill tumor cells even if the surgeon failed to remove all nodes containing micrometastasis. Thus, the oncolytic activity of OBP-401 may function as a backup safety anti-tumor program.

In conclusion, we have demonstrated that the GFP-expressing telomerase-specific replication-selective adenovirus OBP-401 can be delivered into human tumor cells in regional lymph nodes and replicate with selective GFP fluorescence after injection into the primary tumor in an orthotopic rectal tumor model. The feasibility of original OBP-301 (Telomelysin) for human cancer therapy will be confirmed in clinical trials in the near future. As the safety profiles of these two

viruses are considered similar, this molecular imaging strategy using OBP-401 has a potential of being widely available in humans as a novel navigation system in the surgical treatment of malignancy.

METHODS

Cell culture. The human non-small cell lung cancer cell lines H1299 and H460, the human gastric cancer cell lines MKN28 and MKN45, the human colorectal cancer cell line SW620 and HT-29, the human esophageal cancer cell lines TE8 and T.Tn, and the human prostate cancer cell lines LNCaP and PC-3, the human tongue squamous carcinoma cell lines HSC-3, HSC-4, SCC-4 and SCC-9, the human cervical adenocarcinoma cell line HeLa, the human hepatocellular carcinoma cell line HepG2, the human pancreatic cancer cell line Panc-1, the human mammary gland adenocarcinoma cell line MCF-7, the human osteosarcoma cell line U-2OS (ATCC), the normal human lung fibroblast cell line NHLF, the normal human renal epithelial cell line HRE, the human umbilical vascular endothelial cell line HUVEC (TaKaRa Biomedicals), and the normal human lung diploid fibroblast cell line WI38 (HSRRB) were cultured according to the vendor's specifications.

OBP-401. OBP-401 is a telomerase-specific replication-competent adenovirus variant, in which the hTERT promoter element drives the expression of *E1A* and *E1B* genes

linked with an IRES, and inserted *GFP* gene under the CMV promoter into the E3 region for monitoring viral replication[27, 28]. The virus was purified by ultracentrifugation in cesium chloride step gradients, their titers were determined by a plaque-forming assay using 293 cells, and they were stored at –80°C.

Quantitative real-time PCR analysis. Total RNA from the cultured cells was obtained using the RNeasy Mini Kit (Qiagen). The *hTERT* mRNA copy number was determined by real-time quantitative RT-PCR using a LightCycler instrument and a LightCycler DNA TeloTAGGG Kit (Roche Molecular Biochemicals). DNA was extracted with the QIAamp DNA Mini Kit (Qiagen), and quantitative real-time PCR assay for the *E1A* gene was also performed. The sequences of specific primers used for *E1A* were as follows: sense: 5'-CCTGTGTCTAGAGAATGCAA-3' and antisense: 5'-ACAGCTCAAGTCCAAAGGTT-3'. PCR amplification began with a 600-s denaturation step at 95 °C and then 40 cycles of denaturation at 95 °C for 10 s, annealing at 58 °C for 15 s, and extension at 72 °C for 8 s. Data analysis was performed using LightCycler Software (Roche Molecular Biochemicals). The ratios normalized by dividing the value of untreated cells were presented for each sample.

Fluorescence microscopy. Human cancer cell lines (H1299, SW620, and HT29) and normal cells (NHLF) were infected with either 1 or 10 multiplicity of infection (MOI) of OBP-401 for 2 h *in vitro*. Expression of the *GFP* gene was assessed and

photographed (× 200 magnification) using an Eclipse TS-100 fluorescent microscope (Nikon).

Electron microscopy. Human prostate cancer cell line LNCaP was infected with 10 MOI of OBP-401. Thin sections were cut on coated copper grids and stained with uranyl acetate. The samples were examined and photographed with a Hitachi H-7100 transmission electron microscope.

Immunohistochemistry. Immunohistochemical staining was performed using a Histofine SAB PO kit (Nichirei) according to the instructions provided by the manufacturer. Paired tissues of primary tumors and lymph node metastases were obtained form gastric cancer patients who underwent surgery at Okayama University Hospital. Informed consent was obtained from each patient as approved by the Ethics Review Committee for Clinical Investigation of our institution. Formalin-fixed, paraffin-embedded tissue sections were mounted on silanized slides and deparaffinized. After blocking of nonspecific reactivity with rabbit or goat serum for 10 min at room temperature, sections were incubated overnight at 4 °C with the monoclonal antibody to hTERT (Kyowa Medex). After rinsing, the slides were incubated with biotinylated rabbit antibody to mouse, and then with avidin-biotin-peroxidase complex. Peroxidase activity was determined using DAB/H_2O_2 solution (Histofine DAB substrate kit; Nichirei). The slides were

counterstained with methylgreen with Mayer's hematoxylin.

Animal experiments. The experimental protocol was approved by the Ethics Review Committee for Animal Experimentation of our institution. We produced SW620 and HT29 xenografts on the back in 5-week-old female BALB/c *nu/nu* mice by subcutaneous injection of 5×10^6 SW620 or HT29 cells in 100 μl of Hank's balanced salt solution (HBSS) using a 27-gauge needle. When tumors grew to approximately 6-7 mm in diameter, both tumors were intratumorally injected with OBP-401 (1×10^7 PFU/100 μl). Mice were anesthetized by intraperitoneal injection of pentobarbital (50 mg/kg) and examined for GFP expression. Six mice were used for each tumor cell line. To generate an orthotopic rectal cancer model, female BALB/c *nu/nu* mice were anesthetized and then placed in a supine position. The ano-rectal wall was cut at a length of 7 mm to prevent colonic obstruction resulting from rectal tumor progression. We injected cell suspension of HT29 cells at a density of 5×10^6 cells in 100 μl of Matrigel basement membrane matrix (Becton Dickinson Labware) slowly into the submucosal layer of the rectum through a 27-gauge needle (Fig. 4a). Four weeks later, we injected 1×10^8 PFU/100 μl of OBP-401 directly into the rectal tumors. Mice were sacrificed and their abdominal spaces were examined at laparotomy 5 d after virus injection.

Cooled charged-coupled device (CCD) imaging. *In vivo* GFP fluorescence imaging

was acquired by illuminating the animal with a Xenon 150 W lamp. The re-emitted fluorescence was collected through a long pass filter on a Hamamatsu C5810 3-chip color CCD camera (Hamamatsu Photonics Systems). High-resolution image acquisition was accomplished using an EPSON PC. Images were processed for contrast and brightness with the use of Adobe Photoshop 4.0.1J software (Adobe).

ACKNOWLEDGMENTS

This work was supported in part by grants from the Ministry of Education, Culture, Sports, Science, and Technology of Japan (to T. F. and S. K.); and by grants from the Ministry of Health, Labour, and Welfare of Japan (to T. F.). We thank for K. Nagai and H. Kawamura for the helpful discussion. We also thank Y. Shirakiya and N. Mukai for the excellent technical support.

References

1. Tearney, G.J., *et al. In vivo* endoscopic optical biopsy with optical coherence tomography. *Science* **276**, 2037-2039 (1997).
2. MacDonald, S.L., & Hansell, D.M. Staging of non-small cell lung cancer: imaging of intrathoracic disease. *Eur. J. Radiol.* **45**, 18-30 (2003).
3. Kelloff, G.J., *et al.* Progress and promise of FDG-PET imaging for cancer patient management and oncologic drug development. *Clin. Cancer Res.* **11**, 2785-2808 (2005).
4. McMasters, K.M., *et al.* Sentinel lymph node biopsy for melanoma: controversy despite widespread agreement. *J. Clin. Oncol.* **19**, 2851-2855 (2001).
5. Kuerer, H.M., & Newman, L.A. Lymphatic mapping and sentinel lymph node biopsy for breast cancer: developments and resolving controversies. *J. Clin. Oncol.* **23**, 1698-1705 (2005).
6. Koopal, S.A., *et al.* Frozen section analysis of sentinel lymph nodes in melanoma patients. *Cancer* **89**, 1720-1725 (2000).
7. Tanis, P.J., *et al.* Frozen section investigation of the sentinel node in malignant melanoma and breast cancer. *Ann. Surg. Oncol.* **8**, 222-226 (2001).
8. Gulec, S.A., Su, J., O'Leary, J.P., & Stolier, A. Clinical utility of frozen section in sentinel node biopsy in breast cancer. *Am. Surg.* **67**, 529-532 (2001).

9. Chao, C., *et al.* Utility of intraoperative frozen section analysis of sentinel lymph nodes in breast cancer. *Am. J. Surg.* **182**, 609-615 (2001).

10. Misteli, T., & Spector, D.L. Applications of the green fluorescent protein in cell biology and biotechnology. *Nat. Biotechnol.* **15**, 961-964 (1997).

11. van Roessel, P., & Brand, A.H. Imaging into the future: visualizing gene expression and protein interactions with fluorescent proteins. *Nat. Cell Biol.* **4**, E15-20 (2002).

12. Ehrhardt, D. GFP technology for live cell imaging. *Curr. Opin. Plant. Biol.* **6**, 622-628 (2003).

13. Yang, M., Baranov, E., Moossa, A.R., Penman, S., & Hoffman, R.M. Visualizing gene expression by whole-body fluorescence imaging. *Proc. Natl. Acad. Sci. USA* **97**, 12278-12282 (2000).

14. Hasegawa, S., *et al. In vivo* tumor delivery of the green fluorescent protein gene to report future occurrence of metastasis. *Cancer Gene Ther.* **7**, 1336-1340 (2000).

15. Ohtani, S., *et al.* Quantitative analysis of p53-targeted gene expression and visualization of p53 transcriptional activity following intratumoral administration of adenoviral p53 *in vivo*. *Mol. Cancer Ther.* **3**, 93-100 (2004).

16. Kawashima, T., *et al.* Telomerase-specific replication-selective virotherapy for human cancer. *Clin. Cancer Res.* **10**, 285-292 (2004).

17. Taki, M., *et al.* Enhanced oncolysis by a tropism-modified telomerase-specific

replication selective adenoviral agent OBP-405 ("Telomelysin-RGD"). *Oncogene* **24**, 3130-3140 (2005).

18. Umeoka, T., *et al.* Visualization of intrathoracically disseminated solid tumors in mice with optical imaging by telomerase-specific amplification of transferred green fluorescent protein gene. *Cancer Res.* **64**, 6259-6265 (2004).

19. Gu, J., Andreeff, M., Roth, J.A., & Fang, B. hTERT promoter induces tumor-specific Bax gene expression and cell killing in syngenic mouse tumor model and prevents systemic toxicity. *Gene Ther.* **9**, 30-37 (2002).

20. Tsutsumi, S., Kuwano, H., Morinaga, N., Shimura, T., & Asao, T. Animal model of para-aortic lymph node metastasis. *Cancer Lett.* **169**, 77-85 (2001).

21. Maehara, Y., *et al.* Clinical significance of occult micrometastasis in lymph nodes from patients with early gastric cancer who died of recurrence. *Surgery* **119**, 397-402 (1996).

22. Coello, M.C., Luketich, J.D., Litle, V.R., & Godfrey, T.E. Prognostic significance of micrometastasis in non-small-cell lung cancer. *Clin. Lung Cancer* **5**, 214-225 (2004)

23. Fujiwara, T., *et al.* Multicenter phase I study of repeated intratumoral delivery of adenoviral p53 (ADVEXIN) in patients with advanced non-small cell lung cancer. *J. Clin. Oncol.* (in the press).

24. Hiyama, K., *et al.* Activation of telomerase in human lymphocytes and hematopoietic progenitor cells. *J. Immunol.* **155**, 3711-3715 (1995).

25. Adams, J.Y., *et al.* Visualization of advanced human prostate cancer lesions in living mice by a targeted gene transfer vector and optical imaging. *Nat. Med.* **8**, 891-897 (2002).

26. Yang, M., Luiken, G., Baranov, E., & Hoffman, R.M. Facile whole-body imaging of internal fluorescent tumors in mice with an LED flashlight. *Biotechniques* **39**, 170-172 (2005).

27. Watanabe, T., *et al.* Histone deacetylase inhibitor FR901228 enhances the antitumor effect of telomerase-specific replication-selective adenoviral agent OBP-301 in human lung cancer cells. *Exp. Cell Res.* **312**, 256-265 (2006).

28. Fujiwara, T., *et al.* Enhanced antitumor efficacy of telomerase-selective oncolytic adenoviral agent OBP-401 with docetaxel: Preclinical evaluation of chemovirotherapy. *Int. J. Cancer* (in the press).

Figure Legends

Fig. 1 hTERT levels and selective replication of OBP-401 in human cancer cells. (**a**) Relative *hTERT* mRNA expression in human tumor and normal cell lines determined by real-time RT-PCR analysis. The *hTERT* mRNA expression of H1299 human lung cancer cells was considered as 1.0 and the relative expression level of each cell line was calculated against that of H1299 cells. (**b**) Immunohistochemical analysis of the hTERT protein expression in surgical specimens of human gastric cancer and their microscopic metastases in lymph nodes. Representative microscopic images of primary tumor (left panel) and metastatic foci in lymph node (middle and right) are shown. Positive staining is reddish-brown. Counterstain is blue-purple. The original magnification is × 200 (left and middle) and × 400 (right). Scale bar, 100 μm. (**c**) Schematic DNA structures of OBP-401. (**d**) Assessment of viral DNA replication in H1299, SW620, and NHLF cells. Cells were infected with OBP-401 at an MOI of 10 for 2 h. Following the removal of virus inocula, cells were further incubated for the indicated time periods, and then subjected to real-time quantitative PCR assay. The amounts of viral E1A copy number are defined as the fold increases for each sample relative to that at 2 h (2 h equals 1). (**e**) Relationship between viral replication and *hTERT* expression determined by real-time RT-PCR analysis. Plots represent the relative *E1A* DNA levels at 24 h after OBP-401 infection and the relative *hTERT* mRNA levels in SW620, LNCaP, and MCF-7 cell lines. The slope represents the

positive correlation between these two factors ($R^2 = 0.9951$).

Fig. 2 Selective visualization of human cancer cells *in vitro*. H1299 (**a**), SW620 (**b**), HT29 (**c**), and NHLF (**d**) cells were infected with OBP-401 at 1 or 10 MOI for H1299, and 10 MOI for other cell lines. Cell morphology was evaluated at indicated time points by phase-contrast photomicrography (top panels). Cells were also assessed for GFP expression under fluorescence microscopy (bottom panels). × 200 magnification. (**e**) Transmission electron microscopy of LNCaP human prostate cancer cells infected with OBP-401 at an MOI of 10. Black dots represent replicating virus particles.

Fig. 3 Selective visualization of subcutaneous tumors *in vivo*. (**a**) Time course of external images of subcutaneous SW620 and HT29 tumors after intratumoral injection of OBP-401. When tumors grew to approximately 6-7 mm in diameter after subcutaneous inoculation of SW620 and HT29 tumor cells (5×10^6 cells/mouse), OBP-401 at the concentrations of 1×10^7 PFU were directly injected into established tumors. The GFP fluorescence intensity was monitored for 7 d under the CCD non-invasive imaging system. Left panels, macroscopic appearance of subcutaneous tumors; right panels, fluorescent detection. (**b**) SW620 tumors were excised 14 d after OBP-401 injection, and then assessed for GFP fluorescence as a whole tumor or cross-sections. Left panels, macroscopic appearance of subcutaneous tumors; right

panels, fluorescent detection. (**c**) Photographs of non-tumor-bearing *nu/nu* mice injected with OBP-401. Mice were subcutaneously injected with 1×10^7 PFU of OBP-401 and documented as photographs for GFP expression 3 d and 6 d after injection. Arrowheads, injected area.

Fig. 4 Orthotopic xenografts of human colorectal cancer cells and selective visualization of lymph node metastasis in two representative mice (Mouse No. 1 and No. 2). (**a**) Diagram of the method used to produce HT29 human rectal tumors in BALB/c *nu/nu* mice. The rectum of mice were inoculated with 5×10^6 HT29 cells. (**b**) Macroscopic appearance of HT29 rectal tumor 4 weeks after tumor inoculation. Mice were sacrificed and subjected to autopsy. Green line, the direction of tumor cross sections. (**c**) Histologic sections stained with hematoxylin and eosin showing local growth of HT29 tumor in the submucosal layer of the rectum. Scale bar, 100 μm. Left, × 40 magnification; middle, detail of the boxed region of left panel, × 400 magnification; right, lymphatic vessel invasion of HT29 tumor cells (arrowhead). × 400 magnification. (**d**) External images of orthotopic HT29 tumor-bearing *nu/nu* mice injected with OBP-401. OBP-401 at the concentrations of 1×10^8 PFU were directly injected into implanted HT29 tumor (left). The GFP fluorescence could be detected as early as 24 h after OBP-401 injection under CCD imaging. Macroscopic and fluorescent images of HT29 tumor without OBP-401 injection (right). (**e**) Gross appearance of the abdominal cavity (Mouse No. 1). Five days after intratumoral

injection of OBP-401 at the concentrations of 1×10^8 PFU, HT29 tumor-bearing *nu/nu* mice were assessed for lymph node metastasis at laparotomy. The white box outlines a region of (f). (**f**) Three para-aortic lymph nodes were identified in Mouse No. 1 (LN1, LN2, and LN3) (left). Internal imaging with the optical CCD camera visualized one of 3 nodes with GFP fluorescence (LN3) (right). (**g**) Hematoxylin and eosin staining of lymph node sections. Lymph nodes without metastatic tumors (LN1 and LN2). Lymph node containing metastatic tumors (arrowheads) (LN3) (Left, × 200 magnification; right, × 400 magnification). Scale bar, 100 μm. (**h**) Four para-aortic lymph nodes were identified in Mouse No. 2 (LN1, LN2, LN3, and LN4) (left). Three of 4 nodes were positive for light emitting spots with GFP fluorescence (LN1, LN2, and LN3) (right). (**i**) Histopathologic detection of metastatic foci in nodes (LN1 and LN3) (arrowheads).

Table 1 GFP fluorescence and histopathology status in para-aortic lymph nodes of HT29 tumor-bearing mice

Mouse No.	Metastasis[a]	GFP Fluorescence[b]		Total (%)[c]
		Positive	Negative	
No. 1	Positive	1	0	1 (33.3)
	Negative	0	2	2 (66.6)
No. 2	Positive	3	0	3 (75.0)
	Negative	0	1	1 (25.0)
No. 3	Positive	1	0	1 (33.3)
	Negative	0	2	2 (66.6)
No. 4	Positive	0	0	0 (0)
	Negative	0	4	4 (100)
No. 5	Positive	1	1	2 (66.6)
	Negative	0	1	1 (33.3)
No. 6	Positive	3	0	3 (60.0)
	Negative	1	1	2 (40.0)
No. 7	Positive	3	0	3 (50.0)
	Negative	1	2	3 (50.0)

[a]Metastatic foci were detected histologically by hematoxylin and eosin staining.

[b]Nodes with light emitting spots and GFP fluorescence were evaluated as positive.

[c]The percentage of nodes with or without histologically confirmed metastasis in each mouse.

Fig. 1

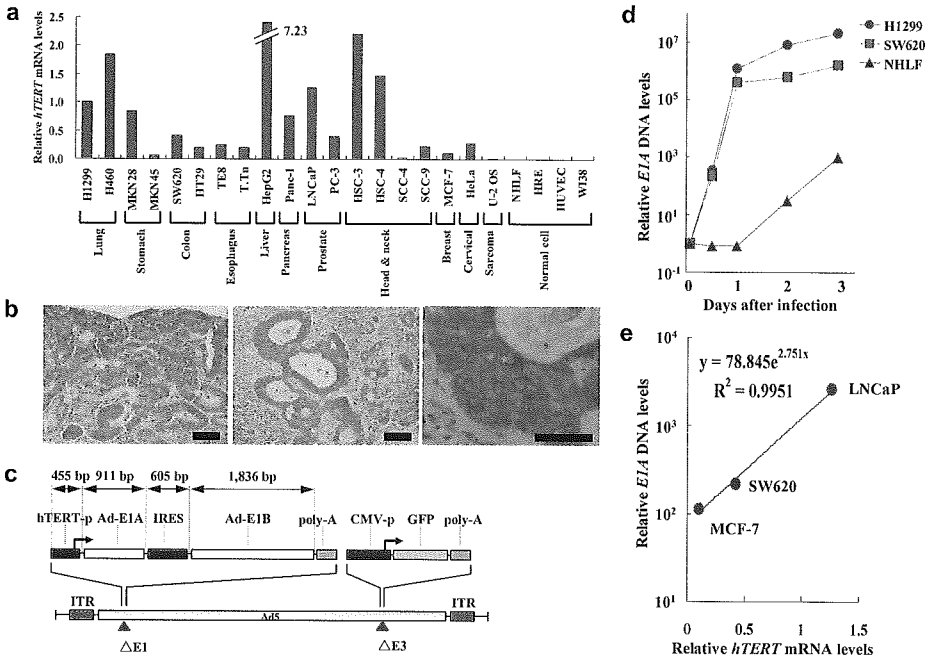
a
Relative hTERT mRNA levels
7.23
H1299
H460
MKN28
MKN45
SW620
HT29
TE8
T-Tn
HepG2
Panc-1
LNCaP
PC-3
HSC-3
HSC-4
SCC-4
SCC-9
MCF-7
HeLa
U-2 OS
NHLF
HRE
HUVEC
WI38
Lung
Stomach
Colon
Esophagus
Liver
Pancreas
Prostate
Head & neck
Breast
Cervical
Sarcoma
Normal cell
b
c
455 bp
911 bp
605 bp
1,836 bp
hTERT-p
Ad-E1A
IRES
Ad-E1B
poly-A
CMV-p
GFP
poly-A
ITR
ITR
Ad5
△E1
△E3
d
Relative E1A DNA levels
H1299
SW620
NHLF
Days after infection
e
y = 78.845e^2.751x
R^2 = 0.9951
LNCaP
SW620
MCF-7
Relative E1A DNA levels
Relative hTERT mRNA levels

Fig. 2

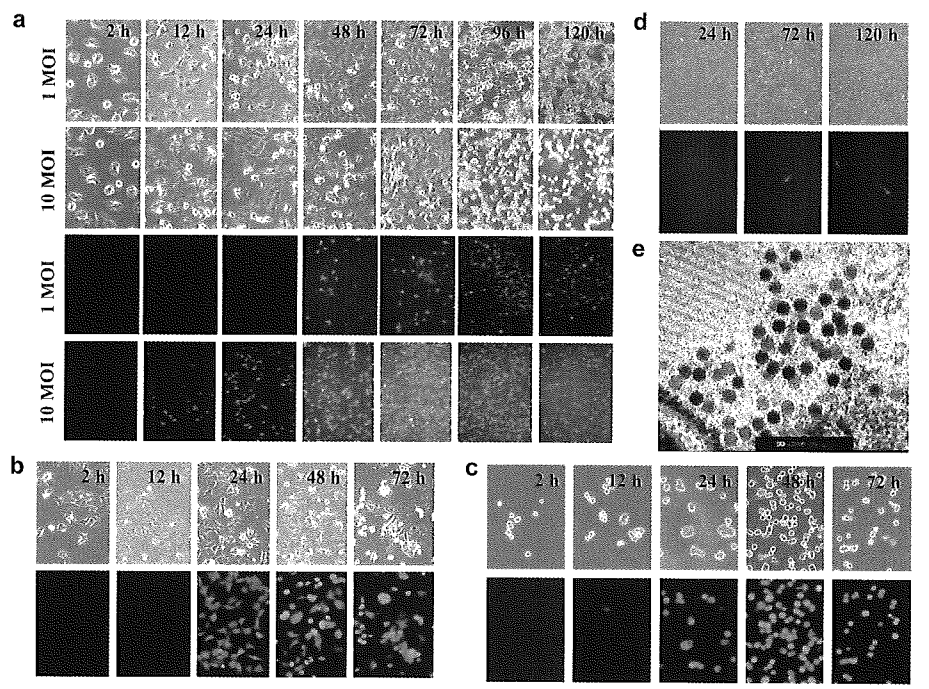
a
2 h
12 h
24 h
48 h
72 h
96 h
120 h
1 MOI
10 MOI
1 MOI
10 MOI
d
24 h
72 h
120 h
e
b
2 h
12 h
24 h
48 h
72 h
c
2 h
12 h
24 h
48 h
72 h